J Solid State Electrochem (2015) 19:1501–1509
DOI 10.1007/s10008-015-2739-5

ORIGINAL PAPER

Improved lithium oxygen battery performance by addition of palladium nanoparticles on manganese oxide nanorod catalysts

Awan Zahoor · Maria Christy · Jeong Sook Jeon · Yun Sung Lee · Kee Suk Nahm

Received: 19 October 2014 / Revised: 30 December 2014 / Accepted: 4 January 2015 / Published online: 3 February 2015

Abstract The need for an alternative electrocatalyst to replace Pt-based noble materials is a major concern of the Li–air battery technology. In this work, α-MnO_2 nanorods are synthesized by a simple hydrothermal technique and are modified with palladium (Pd) nanoparticles to form Pd-deposited α-MnO_2 (Pd/α-MnO_2) nanostructures. The physical characteristics of the thus prepared materials are analyzed by X-ray diffraction (XRD), SEM, and Brunauer–Emmett–Teller (BET) techniques. These analyses confirmed the successful synthesis of 8~10-nm-sized Pd nanoparticles deposited on 82~85-nm-sized α-MnO_2 nanorods. The catalytic activities of the synthesized Pd/α-MnO_2 nanostructure for oxygen reduction reaction and evolution reaction were studied by measuring linear sweeping voltammograms in aqueous solution. The as-prepared material exhibited high electrocatalytic activities which were comparable to that of the commercial Pt/C catalysts. The Pd/α-MnO_2 nanostructures were then examined as a bifunctional electrocatalyst in the air cathode of Li–air batteries in non-aqueous media. The Li–air batteries fabricated with the Pd/α-MnO_2 catalyst deliver a high discharge capacity with low overpotential compared to the other batteries without Pd deposition or any catalyst.

Keywords Air cathode · Electrocatalyst · Manganese oxides · Metal deposition · Palladium nanoparticles · Oxygen reduction

A. Zahoor · K. S. Nahm
School of Semiconductor and Chemical Engineering, Chonbuk National University, Jeonju 561-756, Republic of Korea

M. Christy · K. S. Nahm
R&D Education Centre for Fuel Cell Materials & Systems, Chonbuk National University, Jeonju 561-756, Republic of Korea

J. S. Jeon · K. S. Nahm (✉)
Department of Energy Storage and Conversion, Chonbuk National University, Jeonju 561-756, Republic of Korea
e-mail: nahmks@jbnu.ac.kr

Y. S. Lee (✉)
Faculty of Applied Chemical Engineering, Chonnam National University, Gwangju 500-757, Republic of Korea
e-mail: leeys@chonnam.ac.kr

Introduction

As the demand of clean energy technology grows to an alarming level, the Li–air battery is receiving significant attention because of its tremendous energy storage capacity [1–4]. But there are various crucial problems to be solved for the practical application of the Li–air battery technology. Especially, the slow oxygen reduction reaction kinetics on the cathode is a typical factor to reduce the battery performance [5–9]. These problems directly result in the high cathodic overpotential leading to poor discharge performances and cycleability which narrows down to low gravimetric energy and power densities of the battery [10]. So the development of a new suitable electrocatalyst is essential in the air cathode to improve the reaction kinetics and to solve these problems. So far, various noble metals, alloys, transition metal oxides, nitride, etc. are being investigated as electrocatalysts for air cathodes of Li–air batteries [10–14]. Among them, MnO_2 is found to be one of the best-suited bifunctional electrocatalyst with its non-toxic environmentally friendly nature, abundance, and unique electrochemical properties [15, 16].

MnO_2 is an interesting material with different crystalline structures, whose electrocatalytic activity also varies according to its crystal structure and morphology [17]. In order to understand the relation between their structure and

electrochemical activity, we investigated different MnO_2 nanostructures with different crystalline phases and morphologies as bifunctional electrocatalysts for oxygen reduction reactions (ORR) [18]. We also did a comparative analysis of these MnO_2 electrocatalysts on the air cathode of the Li–air battery and obtained enhanced reaction kinetics with low overpotential resulting in improved overall battery performance [19]. Among all MnO_2 nanostructures, α-MnO_2 exhibited better ORR kinetics with its 2× 2 tunnel structure and delivered a high discharge capacity, double that of the original discharge capacity produced without any electrocatalysts [18, 19]. Other recent reports also support the fact that α-MnO_2 with its unique nanostructure is one of the promising materials for many catalytic applications [17–21]. However, the intrinsically low electronic conductivities of MnO_2 tend to have a limitation in electrochemical performances which are still below those of the commercial Pt/C-based electrocatalysts.

In order to improve the performance of the MnO_2 catalyst, we utilize a common idea of surface modification by depositing metal nanoparticles on its surface. By depositing metal nanoparticles on MnO_2 nanostructures, the overall reaction surface area will increase, resulting in the improved electrocatalytic activity. A recent theoretical investigation also suggests that Pd may allow the possibility of low charging overpotential in the Li–air battery by involving Li_2O_2 facets as main reaction spots, indicating that an effective electrocatalyst can substantially improve the electrochemical performance [22, 23]. Recently, palladium (Pd) nanoparticle catalysts have shown ORR activities similar to that of the commercial Pt/C catalyst and are considered to be promising replacements for the Pt noble catalyst [24, 25]. Also, the strong interaction between MnO_2 and Pd has been shown to increase the catalytic activity of carbon monoxide (CO) oxidation [25, 26]. So in this work, we deposited Pd metal nanoparticles on α-MnO_2 metal oxide nanorods and investigated their electrocatalytic activity with Li–air batteries. Few works have been already reported for the effect of Pd/α-MnO_2 nanorods on Li–air batteries [27–30]. But still, there are lots of different aspects to be explored in order to make this combination possible.

In this work, we have successfully deposited Pd nanoparticles on α-MnO_2 nanorods by a simple and cost-effective two-step process. Initially, α-MnO_2 nanorods were synthesized by a hydrothermal technique, followed by the deposition of Pd on the surface of α-MnO_2 nanorods at room temperature. The electrocatalytic properties of the thus prepared Pd/α-MnO_2 nanorods for oxygen reduction and evolution reactions were evaluated in alkaline media using a linear sweep voltammetry. The Pd/α-MnO_2 nanorods were then employed as an air cathode catalyst in non-aqueous lithium–air battery to investigate the battery performance.

Material and methods

Synthesis of α-MnO_2 nanorods

All chemicals were of analytical grade and were used as received without any further purification. The nanorod-shaped α-MnO_2 nanoparticles were synthesized by a low-temperature hydrothermal technique [9, 10]. In a typical synthesis of α-MnO_2 nanorods, 42 mmol of $KMnO_4$ and 4.2 mL of HNO_3 were added to 50 mL of deionized water under magnetic stirring to form the precursor solution. After stirring for about 30 min, the solution was transferred into a teflon-lined stainless steel autoclave and kept in an electric oven at 120 °C for 12 h. The autoclave was then cooled down at room temperature; the product was filtered, washed with distilled water, and dried at 80 °C for 12 h under vacuum. The final product α-MnO_2 nanorods were collected and confirmed by structural and morphological characterizations.

Deposition of Pd nanoparticles on α-MnO_2 nanorods

The sensitizing solution was prepared by dissolving 0.2 g of $SnCl_2{\cdot}2H_2O$ in 30 mL of deionized (DI) water, and 0.15 g of α-MnO_2 nanorods was dispersed in the solution under stirring condition for 30 min [31, 32]. During the sensitizing process, reductive Sn^{2+} gets adsorbed on the surface of α-MnO_2 which facilitates the deposition of Pd nanoparticles. The sensitized MnO_2 was separated and washed with DI water and dispersed into 30 mL of water to form a suspension. Four milliliters of aqueous solution containing 0.015 g of $PdCl_2$ was added dropwise into the MnO_2 nanorod suspension. Forty milliliters of 0.05 M citric acid was added into the $PdCl_2/MnO_2$ aqueous solution. The pH was adjusted to 8 by adding 1 M KOH solution. $NaBH_4$ was used as a reducing agent. After 4 h, the product was filtered and washed with DI water. The prepared samples were dried overnight in a vacuum oven at 80 °C.

Characterization techniques

The phase structures of the as-prepared samples were determined by powder X-ray diffraction, (XRD, Shimadzu XRD-6000, Cu KR, λ 1.5406 Å) at a scanning rate of 1 °C min^{-1}. The morphology of the as-prepared samples was examined with field emission scanning electron microscopy (FESEM, JSM-6700F), and the chemical composition of the sample was investigated with energy-dispersive X-ray spectroscopy (EDX). The surface area properties were determined by N_2 adsorption/desorption (BELSORP, Bel Japan, Inc.). All the

samples were degassed for 3 h at 300 °C under vacuum before surface area measurements.

Electrocatalytic measurements for oxygen reduction and evolution reactions (ORR and OER) were carried out on a computerized potentiostat instrument (model CHI700C) at room temperature in a three-electrode system using 0.1 M KOH as electrolyte. To measure the ORR and OER polarization curves, the LSV was recorded with a rotating ring glassy carbon disk electrode (RRDE, 5.61 mm in diameter) as the working electrode, in the oxygen-saturated 0.1 M KOH solution at a scan rate of 5 mV s^{-1}, with a disk rotation rate of 1600 rpm. The ORR and OER polarization curves were obtained in the potential ranges of 0.3~−0.8 and 0.3~1.0 V, respectively.

Lithium–air battery applications were studied by a Swagelok™-type cell with a Li metal anode, lithium bis(trifluoromethane sulfonyl) imide (LiTFSI) (tetraethylene glycol dimethyl ether, TEGDME) (1:1) electrolyte, and Ketjen black (KB) cathode with Pd/α-MnO_2 nanorods as catalyst. Each cell was assembled in an argon-filled glove box under room temperature and purged with oxygen before cycle performance. The charge–discharge profiles of the cells were tested in the BTS 2000 (Japan) system at 1 atm O_2 atmosphere.

Preparation of the electrode

For ORR studies, the synthesized Pd/α-MnO_2 nanorods were mixed with carbon powder (Cabot VULCAN XC-72) in the weight ratio of 3:7 to ensure sufficient electronic conductivity. Five milligrams of the as-prepared catalyst was dispersed ultrasonically in 75 μL of diluted Nafion alcohol solution (5 wt%), and about 20 μL of the suspension was pipetted onto a glassy carbon substrate. Pt wire and Hg/HgO were used as the counter and the reference electrode, respectively. Prior to measurement, O_2 was bubbled directly into the cell for at least 1 h.

For lithium–air battery studies, the air cathodes were prepared by mixing an as-prepared Pd/α-MnO_2 nanorod catalyst and Ketjen black (EC 600JD) conductive carbon in the ratio of 1:2 with teflonized acetylene black (TAB) binder (60 %) in isopropyl alcohol. The mixture was prepared into a fine pellet of about 1 cm diameter, and the pellet was pressed on a Ni mesh current collector with a diameter of 1.2 cm. Thus, the prepared electrode is then dried in vacuum overnight at 100 °C and used as air cathode in the Li–air battery.

Fabrication of a Li–O_2 battery

The Li–O_2 cell performance was tested galvanostatically under oxygen flow (10 cc min^{-1}) in a potential window of 2~4.3 V in a BTS 2004 (Japan) battery tester at different current densities (0.1–0.3 mA cm^{-2}). The performance of the Pd/α-MnO_2 nanorod catalyst in the Li–O_2 air cathode was evaluated using the Swagelok™-type cells. Li foil was used as the anode, our prepared electrode (as mentioned above in "Preparation of the electrode") was used as the cathode, and 1 M LiTFSI (TEGDME) was employed as the electrolyte. The TEGDME-based electrolyte has been used in this study because it has been reported to be relatively stable, less volatile, and more conductive than other carbonate-based electrolytes in air batteries [6, 33–38]. These electrolytes are also reported to possess substantially higher stability than carbonates as they are less susceptible to nucleophilic substitution by the superoxide anion radical [35] and are stable against oxidation potentials up to 4.5 V versus Li/Li^+ unless in the presence of Li_2O_2 [36–39]. We have utilized a potential window of 2~4.3 V in this study mainly because the decomposition voltage of TEGDME was determined to be above 4.3 V [38]. Another main important point is that the discharge and charge reactions in the Li–O_2 battery can be expressed as ($2Li^+ + O_2 + 2e^- \leftrightarrow Li_2O_2$), and Li_2O_2 is found to be the main discharge product in TEGDME-based electrolytes without any side reactions/products.

Results

Physical properties

The X-ray diffraction patterns for the synthesized nanorods are given in Fig. 1. The peaks at 13°, 18°, 27°, 36°, 42°, 48°, 59°, and 65° are characteristic ones for the α-MnO_2 phase indexed to tetragonal α-MnO_2 structures (JCPDS 44-0141),

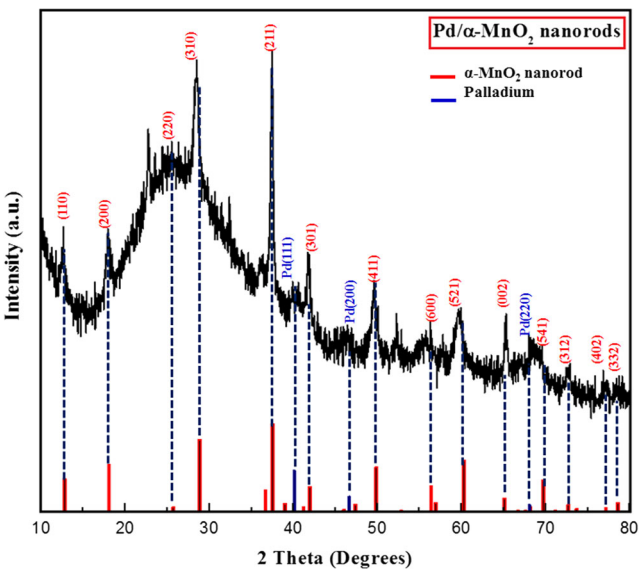

Fig. 1 XRD spectra of synthesized Pd-deposited α-MnO_2 nanorods

and the peaks at 40°, 46°, and 67° correspond to the Pd (1 1 1), (2 0 0), and (2 2 0) planes. Figure 1 clearly shows that the synthesized nanorods are composed of α-MnO_2 and they are decorated with Pd nanoparticles with no other impurities to show [25, 40]. The lattice parameters for α-MnO_2 were also calculated by Rietveld analysis and found to be a=0.98 and c=0.28 nm comparable to that of standard values [19, 40].

The morphology of synthesized α-MnO_2 was examined by FESEM images, given in Fig. 2a together with a high-magnification image (inset). The image clearly shows the formation of nanorod structures that are densely and randomly aligned. The diameter of the nanorods varies from 82 to 85 nm with average length of 1–1.5 μm. The smooth surfaces of the MnO_2 nanorods can be clearly seen without any defects. Figure 2b shows the SEM and high-magnification image (inset) of Pd/α-MnO_2 nanorods. The average diameter of the Pd nanoparticle estimated from the FESEM image is about 8~10 nm. From the FESEM image, it can be observed that Pd nanoparticles are homogenously distributed over α-MnO_2 nanorods. After confirming the deposition of Pd nanoparticles on α-MnO_2 by XRD spectra and SEM images, the samples were subjected to EDX analysis to find out the amount of Pd deposition. According to EDX mapping shown in Fig. 2c and elemental analysis details given in Fig. 2d as inset Table 1, the average weight of Pd nanoparticles deposited on α-MnO_2 nanorods is about ~2.4 weight percentage.

The Brunauer–Emmett–Teller (BET) surface area analyses of the synthesized materials are given in Fig. 3, and the surface properties are included in the inset Table 2. From the table, the specific surface area of the synthesized Pd/α-MnO_2 nanorods is found to be 70 $m^2\ g^{-2}$, which is better than that of the α-MnO_2 nanorods which is 25 $m^2\ g^{-1}$. The type IV characteristics observed from the N_2 adsorption desorption isotherm shown in Fig. 3 show the mesoporosity of the synthesized material which is also better than the simple α-MnO_2 nanorods. The vertical shift in the location of the hysteresis loop to higher volumes of nitrogen gas adsorption indicates the enhanced porosity in the Pd-added sample. Similarly, from Table 2, it can be seen that the pore size and pore volume have also increased greatly after Pd deposition on α-MnO_2 than simple α-MnO_2 nanorods. The Pd deposition on α-MnO_2 nanorods has significantly enhanced the surface and pore properties of the materials.

Electrocatalytic properties of Pd/α-MnO_2 nanorods

To investigate the electrocatalytic activities of the Pd/α-MnO_2 nanorods, ORR were examined by LSV in O_2-saturated 0.1 M

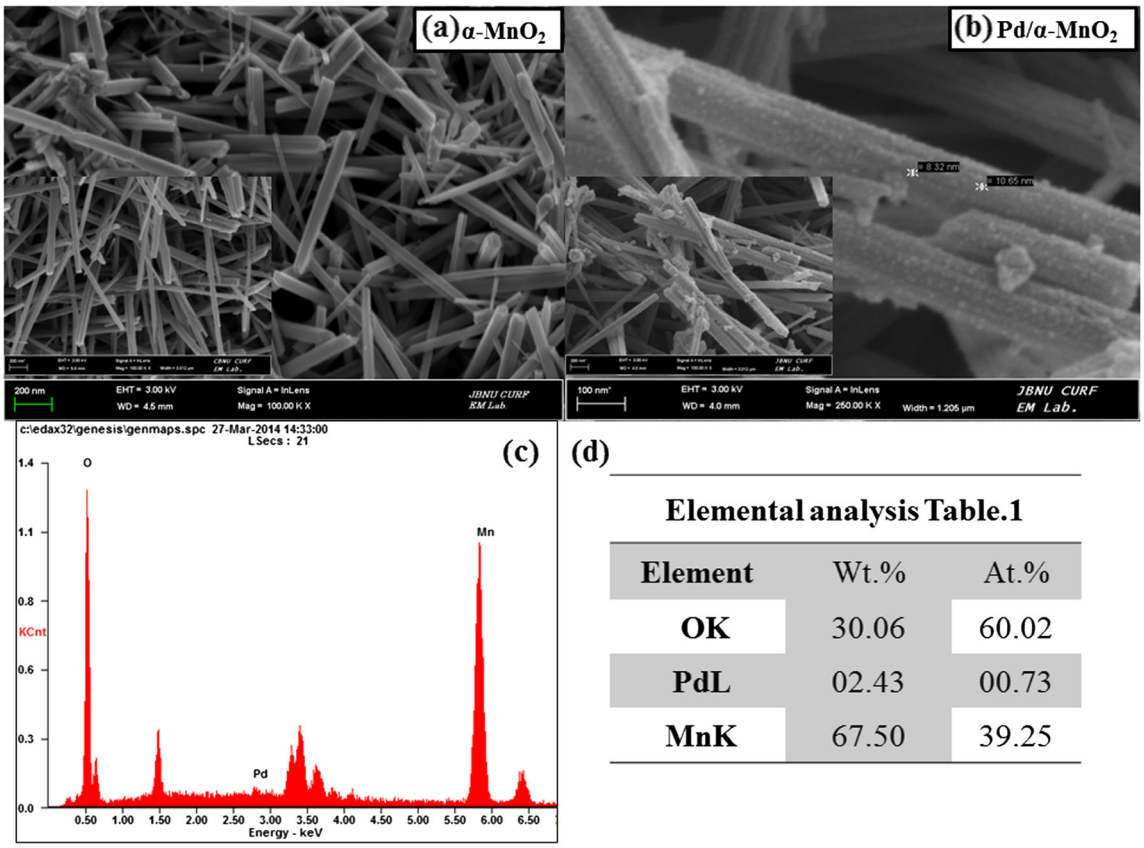

Fig. 2 FESEM images of **a** α-MnO_2 nanorods and **b** Pd-deposited α-MnO_2 nanorods (*insets* show high-resolution images); **c** EDX spectra of synthesized Pd-deposited α-MnO_2 nanorods and **d** *inset Table 1* showing elemental analysis

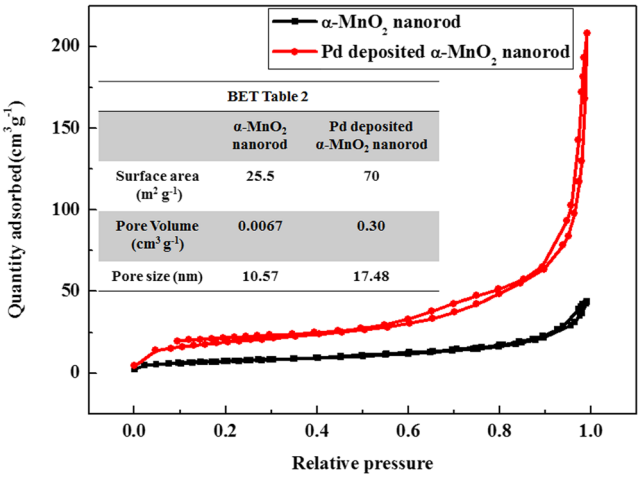

Fig. 3 N_2 adsorption/desorption isotherm of Pd-deposited α-MnO_2 nanorod-catalyzed Li–O_2 battery in comparison with α-MnO_2 nanorods (*inset Table 2* gives specific values derived from Fig. 3)

KOH solution at a scan rate of 5 mV s^{-1} with the disk rotation rate of 1600 rpm. For comparison, LSV was also performed on commercial 20 wt% Pt/C and α-MnO_2 nanorods under the same experimental conditions. The LSV data for all the measured materials were obtained in the potential range of 0.3~−0.8 V and are given in Fig. 4. The onset potential, mass activity, and the number of electron transfer were calculated from the LSV data as shown in the inset Table 3 (included in Fig. 4). The onset potential of Pd/α-MnO_2 nanorods is −0.003 V which is more positive than α-MnO_2 nanorods without Pd and almost similar to the onset potential of commercial Pt/C. This shows the enhanced electrocatalytic activity of the Pd/α-MnO_2 catalyst due to the addition of Pd nanoparticles. In addition, the mass activities of the catalysts were calculated with respect to their kinetic current density as given in Table 3 included in Fig. 4. The mass activity of Pd/α-MnO_2 nanorods is much higher than that of the α-MnO_2 with high kinetic current density. These results also confirm that the electrocatalytic activity of α-MnO_2 nanorods has been greatly enhanced by the addition of Pd nanoparticles. The electron transfer number per oxygen molecule (n) during ORR from Fig. 4 was calculated by the equation,

$$n = \frac{4I_D}{I_D + \frac{I_R}{N}} \quad (1)$$

where I_D, I_R, and N are disk current, ring current, and ring collection efficiency (here N=0.37), respectively [39]. The electron transfer number for α-MnO_2 is calculated to be 3.3, while for Pd/α-MnO_2, it is 3.8, which is much higher and

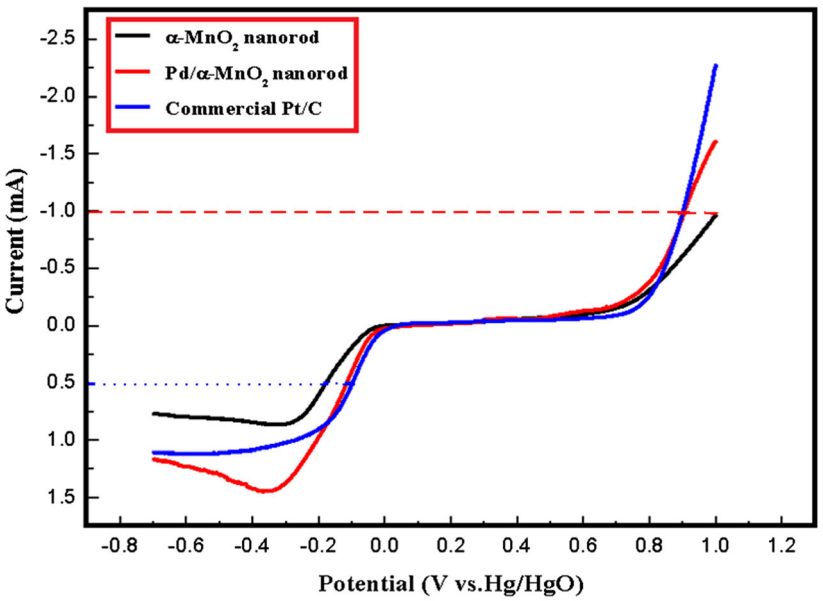

Fig. 4 LSV curves recorded in the oxygen-saturated 0.1 M KOH solution at a scan rate of 5 mV s^{-1} with a disk rotation rate of 1600 rpm. The ORR and OER polarization curves were obtained in the potential ranges of 0.3~−0.8 and 0.3~1.0 V, respectively (*inset Table 3* gives specific values derived from Fig. 4)

Table 3 ORR characteristics derived from Figure 4					Electrochemical properties of the catalysts		
S.NO	Sample	Onset Potential V	Mass activity mA/mg	Electron transfer number	ORR E (V) at I = 0.5 mA	OER E (V) at I = -1.0 mA	Oxygen Electrode Δ (OER - ORR) E (V)
1	α–MnO_2	-0.005	22	3.3	-0.18	1.00	1.18
2	Pd /α–MnO_2	-0.003	57	3.8	-0.11	0.89	1.00
3	Commercial Pt/C	-0.003	93	3.9	-0.09	0.89	0.98

closer to the commercial Pt/C catalyst with an n value of 3.9. This value (close to 4) is much preferable for ORR because of its one-step direct four-electron transfer mechanism [41], and our experimental results show that Pd/α-MnO_2 is such a bifunctional catalyst that promotes the direct mechanism. It has also been experimentally verified by other reports that Pd nanoparticles mainly catalyze a direct four-electron transfer reaction [25, 29]. Shao et al. [42] have also explained the ORR characteristics of Pd and mentioned them as relatively reactive materials. Pd oxidizes at more negative potentials than Pt and is positioned on the ascending branch of the ORR plot right below Pt [42–45]. Also, Mn has $4s^2$ and $3d^5$ in its valence orbital whereas Pd has a fully occupied d orbital. According to Wang et al. [45], when two such orbitals with low d band occupancy and fully occupied d band are coupled, ORR would be enhanced. Thus, in this case, the combination of Pd and α-MnO_2 greatly enhances the ORR performance in the aqueous medium.

To evaluate the ability to catalyze OER, we measured the polarization curves on the LSV during the anodic potential scan in the range of 0.3~1.0 V versus Hg/HgO in 0.1 M KOH solution at a scan rate of 5 mV s^{-1} with the disk rotation rate of 1600 rpm, as shown in the right side part of Fig. 4. Interestingly, Pd/α-MnO_2 exhibits OER characteristics better than that of the commercial Pt/C and α-MnO_2 nanorod. This identifies the Pd/α-MnO_2 nanorod bifunctional catalytic behavior. Table 3 also quantitatively compares the bifunctional oxygen electrode activity of Pd/α-MnO_2 to those of the α-MnO_2 nanorod and commercial Pt/C. Figure 4 is used to quantify the ORR and OER for the synthesized materials. The potential at which the current reaches half of its maximum value (half-wave potential) was selected for the ORR activities of the samples. Therefore, an ORR current of 0.5 mA was selected, which approximates the half-wave potential. Activities for the OER were judged by the potential required to oxidize water at a current of −1.0 mA, a convention commonly used in the OER literature [46]. To assess the overall oxygen electrode activity, the difference between the ORR and the OER was tabulated. The smaller the difference, the closer the catalyst is to an ideal reversible oxygen electrode. From Table 3, the Pd/α-MnO_2 catalyst has an oxygen electrode activity of 1.0 V, which is almost comparable to that of commercial Pt/C.

Li–air battery performance

The Swagelok™-type cells were assembled to investigate the catalytic effect of the Pd/α-MnO_2 nanorod on the air cathode of the Li–air battery. We examined and compared the catalytic activity of three electrodes without any catalyst and with catalysts, namely, Pd/α-MnO_2 and α-MnO_2, and observed the performance of the Pd/α-MnO_2-catalyzed electrode with respect to the other two electrodes. The KB–air cathode with and without catalysts was tested versus the (Li/Li^+) lithium metal anode for cycling performance, and their gravimetric charge–discharge profiles are given in Fig. 5. The batteries were tested at a constant current density of 0.1 mA cm^{-2} in the potential range 2.0–4.3 V at room temperature and O_2 atmosphere. From Fig. 5a, it can be clearly seen that our Pd/α-MnO_2 nanorod catalyst has exhibited a significantly high specific capacity in the first cycle. The first discharge curve of Pd-deposited α-MnO_2 nanorods reached a maximum capacity of 8526 mAh g^{-1} with a flat discharge plateau at 2.7 V. On charging, a maximum capacity of 8526 mAh g^{-1} at 4.3 V is obtained with maximum reversibility. In addition, the difference in the discharge and charge potential or overpotential, ΔV, is 1.0 V which is very low and favorable for the reversibility of the battery. This means that the Pd/α-MnO_2 nanorod catalyst has efficiently increased the reversibility of the cell. In fact, the obtained capacity is higher than other reports from Pd/α-MnO_2-catalyzed Li–air batteries [27, 28]. For comparison, the cycling data of α-MnO_2 nanorod-catalyzed cells were also measured under the same conditions and are given in Fig. 5a. The first discharge and charge curves of the α-

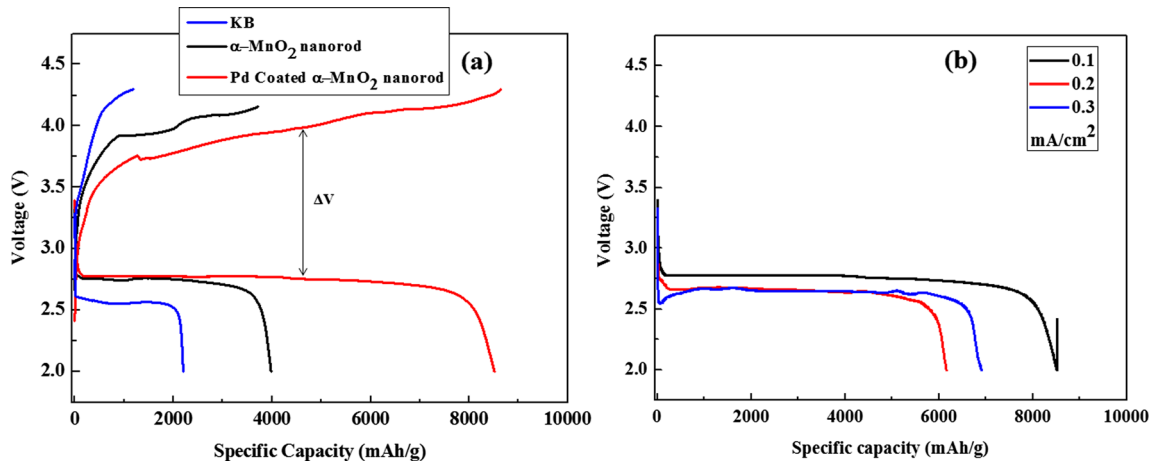

Fig. 5 Charge–discharge profiles of Pd-deposited α-MnO_2 nanorod-catalyzed Li–O_2 battery (**a**) in comparison with α-MnO_2 nanorod- and KB-catalyzed batteries (**b**) at different current densities

MnO_2 nanorod catalyst exhibit a maximum capacity of 3997 (~4000)mAh g^{-1} with an overpotential (ΔV) of 1.36 V. It is clearly seen that the addition of Pd on α-MnO_2 has doubled the specific capacity and reduced the overpotential of the Li–air battery. Also, the specific capacity obtained with our Pd-coated electrocatalyst (8526 mAh g^{-1}) is about four times higher than that of the original capacity of the cells (2000 mAh g^{-1}) without any catalysts (Fig. 5a). This shows that our synthesized Pd/α-MnO_2-catalyzed Li–air batteries show better performance than the other two batteries with only the α-MnO_2 catalyst and without any catalyst. This better performance of the Pd/α-MnO_2 catalyst in non-aqueous phase is in consistence with the better ORR/OER performance in aqueous phase. As it has been concluded from various literatures, most of the catalysts used for ORR/OER in aqueous phase have been efficient catalysts in non-aqueous Li–O_2 batteries as well. Our experiment results suggest that the high specific capacity, reversibility, and low overpotential can be attributed to the α-MnO_2 catalysts especially due to the addition of Pd on α-MnO_2.

A low overpotential clearly means that the air cathode is highly reversible [27–30]. To test the reversibility of the Pd/α-MnO_2 electrocatalyst on the air cathode, the cells were tested at different current densities. The first cycle discharge capacities of Li–O_2 cells at different current densities are compared in Fig. 5b. From Fig. 5b, we can see that even with higher current densities of 0.2 and 0.3 mA cm^{-2}, a maximum discharge capacity of >6000 mAh g^{-1} is obtained. One of the major drawbacks of the Li–air battery is its poor rate capability which results in a higher discharge capacity only with very low current density. But in this case, we have obtained a good discharge capacity even with a high current density of 0.2 mA cm^{-2}. From the figure, it can be seen that all the first discharge capacities are fairly high with the maximum capacity obtained at 0.1 mA cm^{-2}. However, a fade in capacity was observed after the first cycle not shown in Fig. 5b. The capacity slowly degraded in the subsequent cycles which is generally attributed to the slow oxidation kinetics of Li_2O_2 formed upon discharge [47–49]. To understand this process in detail, the formation decomposition mechanism of Li_2O_2 in the air cathode was investigated in a later section.

To obtain complete stable cycling without any fade in the capacity, we also investigated the cells with limited depth of discharge. Considerable cycling performance can be improved by limiting the depth of discharge and charging [50, 51]. The cycle life and efficiency of the battery were analyzed at a fixed capacity of 500 and 800 mAh g^{-1} (at 0.1 mA cm^{-2}), as given in Fig. 6a, b. From Fig. 6a, it can be seen that uniform cycling at 500 mAh g^{-1} is obtained up to 35 cycles in which an overpotential of 1.2 V is noted for 20 cycles. After 20 cycles, the overpotential increases slowly. Similarly, uniform cycling at 800 mAh g^{-1} as seen in Fig. 6b is obtained up to 20 cycles and with overpotential of 1.2 V for the first 15 cycles.

The improved performance of the Pd/α-MnO_2-catalyzed Li–O_2 cell compared to the other two cells (Fig. 5) can be attributed to the catalyst where both α-MnO_2 and the Pd deposited on the α-MnO_2 contribute beneficially. α-MnO_2 is proven to be beneficial with its 2×2 crystal structure which favors the movement of ions in addition to the OH^- groups which helps in surface adsorption of O_2 and dissociation of O–O bonds [20]. The nanorod structure also helps with the easy deposition of Pd. In addition, the high activity of the synthesized catalyst can be mainly attributed to the Pd nanoparticles deposited on the surface of the MnO_2 nanorods. It is well known that Pd/α-MnO_2 has higher electrocatalytic activity towards ORR when compared to the pure MnO_2 materials [25, 29]. The Li–O_2 battery results confirm the better performance of Pd/α-MnO_2-catalyzed cells than that of α-MnO_2 catalyzed cells or cells without any catalysts. It can be seen that our Pd/α-MnO_2 electrocatalyst also helps in the decomposition of discharge products in addition to its electrocatalytic activity in ORR. That is, Pd/α-MnO_2 has high catalytic activity for both ORR and OER and is suited as a bifunctional electrocatalyst for the Li–air battery [28]. The BET measurement shown in Fig. 3 and Table 2 (inset) also supports the fact that Pd nanoparticles deposited on the surface of the MnO_2

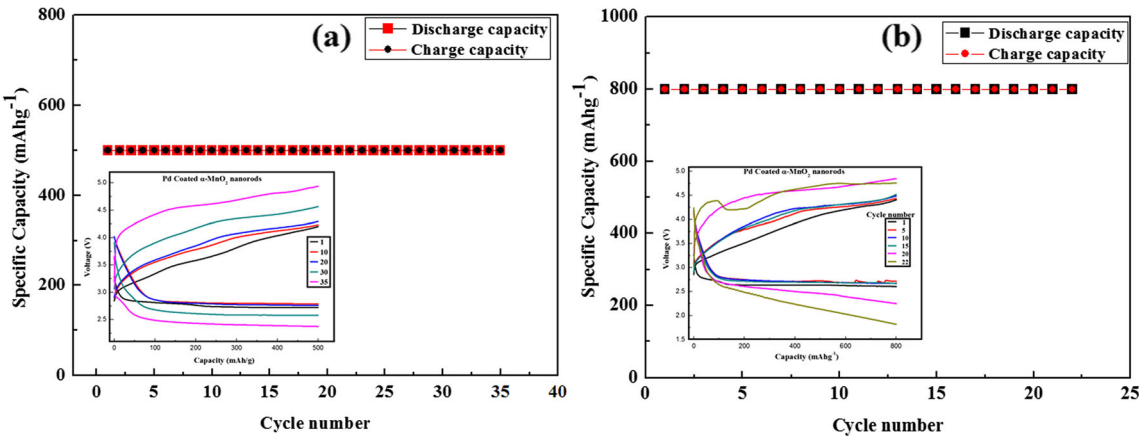

Fig. 6 Cycling characteristics of Pd-deposited α-MnO_2 nanorod-catalyzed Li–O_2 battery at limited depth of discharge **a** 500 and **b** 800 mAh g^{-1}

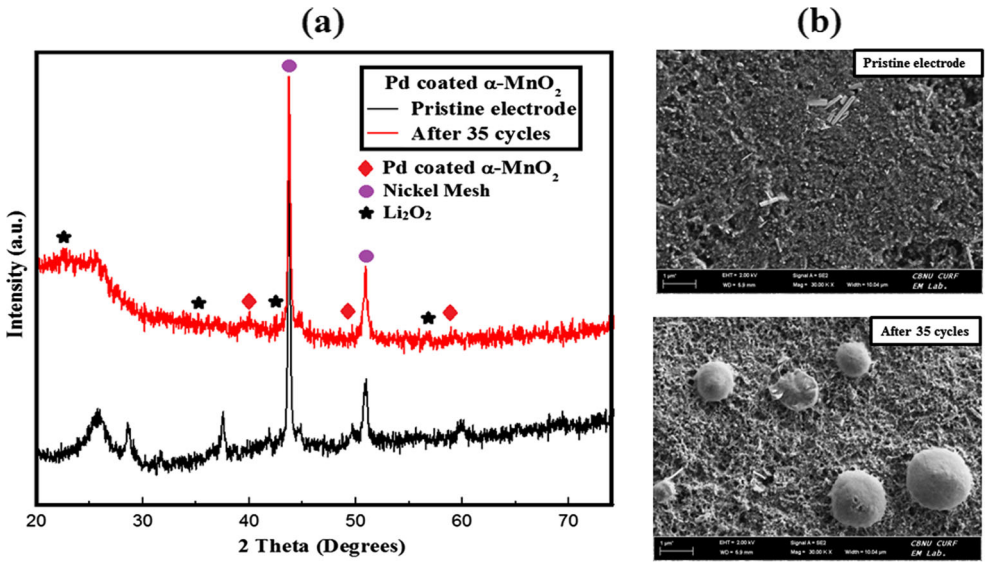

Fig. 7 **a** XRD spectra and **b** FESEM images of Pd-deposited α-MnO_2 nanorod-catalyzed air cathode before (pristine) and after cell cycling

nanorods help to improve the reaction kinetics. From Fig. 3, it is clear that the N_2 adsorption kinetics of Pd/α-MnO_2 is higher than that of α-MnO_2 and they became highly mesoporous after the deposition of Pd. Table 2 shows an increase in surface area, pore volume, and pore size for Pd/α-MnO_2 than simple α-MnO_2. This means that Pd deposition has significantly increased the reaction surface area of our material. So, the high performance of the Pd/α-MnO_2-catalyzed cell can be directly related to the high surface area, pore volume, and pore size of the material.

Post-cycling study on the air cathode

To validate the reversible electrochemical reaction and to analyze the formation of any discharge products during the charge–discharge process, pre- and post-cycling tests were examined on the Pd/α-MnO_2 electrocatalyst-loaded air cathodes. Figure 7a shows the XRD spectra observed from the pristine electrode as prepared and the electrode carefully removed in a glove box after cell cycling tests. The XRD spectra of pristine electrodes show characteristic peaks for Pd, MnO_2, carbon (for KB), and Ni (for Ni mesh current collector). There were no other impurity peaks observed in the electrodes. But the electrodes after cycling show the formation of Li_2O_2. The weak peaks of Li_2O_2 might be due to the fact that the spectrum was observed after complete discharge cycles. However, this makes sure that there are some irreversible discharge products formed on the surface of the electrode after cycling.

To confirm this clearly, an SEM measurement was also taken on the same electrode surfaces. Figure 7b shows the SEM images of the as-prepared pristine electrode surface and the electrode surface after the cycling experiment, respectively. The pristine electrode shows a smooth surface with some visible nanorods. However, the electrode surface after cycling shows the formation of some spherical-like particles of about 1.5–2 μm on the electrode surface. This could be the formation of Li_2O_2 over and over upon discharging which was not reversed back on cycling. The SEM images along with the XRD spectra confirm the formation of irreversible Li_2O_2 during the discharge process, thereby covering the surface of the cathode like a film. The shape of the residue could vary according to the materials used on the electrode materials [52]. On a higher magnification, both Li_2O_2 and small rod structures are visible. So, it must be the formation of these irreversible solid products which blocks the pores on the surface for further formation/decomposition reactions during cycling eventually resulting in the capacity fade in the cell. If Pd/α-MnO_2 is further optimized for its structural stability on cycling, this could be a potential candidate for Li–air battery electrocatalyst [29, 53]. Another possible reason for this capacity degradation might be the decomposition of the electrolyte on prolonged cycling. Nevertheless, our Pd/α-MnO_2 catalyst or the addition of Pd on α-MnO_2 is proven to be the most effective in decreasing the charge potential and delivering a high capacity with capacity retention.

Conclusions

In this work, Pd-deposited α-MnO_2 nanorods were synthesized by a simple two-step process. The as-prepared materials showed very high electrocatalytic activity for ORR and OER in aqueous media comparable to that of commercial Pt/C catalysts. When the developed electrocatalyst was applied to the air cathode in the non-aqueous Li–air battery, it delivered a very high discharge capacity of 8526 mAh g^{-1} with 100 % reversibility in the first cycle. Pd coated on the MnO_2-catalyzed air cathode exhibits low overpotential and better battery

cycling compared to both the α-MnO_2-catalyzed and KB-only air cathodes. This report clearly attests to the efficiency of Pd/α-MnO_2 as a bifunctional electrocatalyst which is highly active for both ORR and OER of rechargeable Li–air batteries.

Acknowledgments This work was supported by the Human Resources Development program (No. 20114030200060) of the Korea Institute of Energy Technology Evaluation and Planning (KETEP) grant funded by the Korea government Ministry of Trade, Industry and Energy. This work is also supported by the Basic Science Research Program through the National Research Foundation (NRF) funded by the Ministry of Education (No. 2013R1A1A2012656).

References

1. Girishkumar G, McCloskey B, Luntz AC, Swanson S, Wilcke W (2010) J Phys Chem Lett 1:2193–2203
2. Park M, Sun H, Lee H, Lee J, Cho J (2012) Adv Energy Mater 2(7): 780–800
3. Bruce PG, Freunberger SA, Hardwick LJ, Tarascon JM (2012) Nat Mater 11:19–29
4. Imanishi N, Yamamoto O (2014) Mater today 17:24–30
5. Zahoor A, Christy M, Hwang YJ, Nahm KS, J Electrochem Sci Technol 3(1):14–23
6. Jung H, Hassoun J, Park J, Sun Y, Scrosati B (2012) Nat Chem 4: 579–585
7. Laoire CO, Mukerjee S, Abraham KM, Plichta EJ, Hendrickson MA (2009) J Phys Chem C 113(46):20127–20134
8. Mo Y, Ong SP, Ceder G (2011) Phys Rev B 84:205446. doi:10.1103/PhysRevB.84.205446
9. Debart A, Bao J, Armstrong G, Bruce PG (2007) J Power Sources 174:1177
10. Horn YS, Park S, Xiao J, Zhang J, Wang Y, Liu (2012) J ACS Catal 2(5):844–857
11. Su D, Kim H, Kim W, Wang G (2013) J Power Sources 244:488–493
12. Thapa A, Shin T, Ida S, Sumanasekera GU, Sunkara MK, Ishihara T J Power Sources 220: 211–216
13. Lu YC, Xu Z, Gasteiger HA, Chen S, Schifferli KH, Horn YS (2010) J Am Chem Soc 132(35):12170–12171
14. Lu YC, Gasteiger HA, Horn YS (2011) J Am Chem Soc 133(47): 19048–19051
15. Oloniyo O, Kumar S, Scott K (2012) J Electron Mater 41(5):921–927
16. Debart A, Paterson AJ, Bao J, Bruce PG (2008) Angew Chem 120: 4597–4600
17. Truong TT, Liu Y, Ren Y, Trahey L, Sun Y (2012) ACS Nano 6(9): 8067–8077
18. Zahoor A, Jeon JS, Jang HS, Christy M, Nahm KS (2014) Science of Advanced Materials
19. Zahoor A, Jang HS, Jeon JS, Christy M, Hwang YJ, Nahm KS (2014) RSC Adv 4:8973–8977
20. Cheng F, Su Y, Liang J, Tao Z, Chen J (2010) Chem Mater 22:898–905
21. Neburchilov V, Wang H, Martin JJ, Qu W (2010) J Power Sources 195:1271–1291
22. Lu J, Lei Y, Lau KC, Luo X, Du P, Wen J, Assary RS, Das U, Miller DJ, Elam JW, Albishri HM, El-Hady D, Sun YK, Curtiss LA, Amine K, Nature commun A nanostructured cathode architecture for low charge overpotential in lithium-oxygen batteries. DOI:10.1038/ncomms3383
23. Thapa A, Hidaka Y, Hagiwara H, Ida S, Ishihara T (2011) J Electrochem Soc 158(12):A1483–A1489
24. Ding K (2010) Int J Electrochem Sci 5:668–681
25. Sun W, Hsu A, Chen R (2011) J Power Sources 196:4491–4498
26. Salker AV, Kunkalekar RK (2009) Catal Commun 10:1776–1780
27. Thapa A, Ishihara T (2011) J Power Sources 196:7016–7020
28. Zhang M, Xu Q, Sang L, Ding F, Liu X, Jiao L (2014) Trans Nonferrous Metals Soc China 24:164–170
29. Jung KN, Riaz A, Lee SB, Lim TH, Park SJ, Song RH, Yoon S, Shin KH, Lee JW (2013) J Power Sources 244:328–335
30. Thapa A, Saimen K, Ishihara T (2010) Electrochem Solid-State Lett 13(11):A165–A167
31. Zhu J, Su Y, Cheng F, Chen J (2007) J Power Sources 166:331–336
32. Niazi AR, Li SK, Wang YC, Liu JX, Hu ZY, Usman Z (2014) Trans Nonferrous Metals Soc China 24:136145
33. Balaish M, Kraytsberg A, Ein-El Y (2014) Phys Chem Chem Phys 16:2801–2822
34. McCloskey BD, Bethune DS, Shelby RM, Girishkumar G, Luntz AC (2011) J Phys Chem Lett 2(10):1161–1166
35. Bryantsev VS, Giordani V, Walker W, Blanco M, Zecevic S, Sasaki K, Uddin J, Addison D, Chase GV (2011) J Phys Chem A 115: 12399–12409
36. McCloskey BD, Scheffler R, Speidel A, Bethune DS, Shelby RM, Luntz AC (2011) J Am Chem Soc 133:18038–18041
37. Bethune DS, Shelby RM, Girishkumar G, Luntz AC, McCloskey BD (2011) J Phys Chem Lett 2:1161–1166
38. Lim HD, Park KY, Gwon H, Hong J, Kim H, Kang K (2012) Chem Commun 48:8374–8376
39. Hou J, Yang M, Ellis MW, Moorec RB, Yid B (2012) Phys Chem Chem Phys 14:13487–13501
40. Wang X, Li Y (2002) J Am Chem Soc 124(12):2880–2881
41. Zahoor A, Christy M, Hwang YJ, Lim YR, Kim P, Nahm KS (2014) Appl Catal B Environ 147:633–641
42. Lu YC, Gasteiger H, Horn YS (2011) J Am Chem Soc 133:19048–19051
43. Peng Z, Freunberger SA, Hardwick LJ, Chen Y, Giordani V, Bardé F, Novák P, Graham D, Tarascon JM, Bruce PG (2011) Angew Chem Int Ed 50:6351–6355
44. Norskov JK, Rossmeisel J, Logadottir A, Lindqvist L, Kitchin JR, Bligaard T, Jonsson H (2004) J Phys Chem B 108:17886–17892
45. Wang YX, Balbuena PB (2005) J Phys Chem B 109:18902–18906
46. Lima FHB, Calegaro ML, Ticianelli EA (2007) Electrochim Acta 52: 3732–3738
47. Ida S, Thapa AK, Hidaka Y, Okamoto Y, Matsuka M, Hagiwara H, Ishihara T (2012) J Power Sources 203:159–164
48. Zhang GQ, Zheng JP, Liang R, Zhang C, Wang B, Au M, Hendrickson M, Plichta EJ (2011) J Electrochem Soc 158:A822–A827
49. Ogasawara T, Debart A, Holzapfel M, Novak P, Bruce PG (2006) J Am Chem Soc 128:1390–1393
50. Padbury R, Zhang X (2011) J Power Sources 196(10):4436–4444
51. Xu D, Wang ZI, Xu JJ, Zhang LL, Zhang XB (2012) Chem Commun 48:6948–6950
52. Han X, Hu Y, Yang J, Cheng F, Chen J (2014) Chem Commun 50: 1497–1499
53. Choi R, Jung J, Kim G, Song K, Kim Y, Jung S, Han Y, Song H, Kang Y (2014) Energy Environ Sci 7:1362–1368